doi:10.1093/brain/awq217 Brain 2010: 133; 3323–3335 | 3323

BRAIN
A JOURNAL OF NEUROLOGY

Blocking ADAM10 synaptic trafficking generates a model of sporadic Alzheimer's disease

Roberta Epis,[1,*] Elena Marcello,[1,*] Fabrizio Gardoni,[1] Csaba Vastagh,[1] Matteo Malinverno,[1] Claudia Balducci,[2] Alessio Colombo,[2] Barbara Borroni,[3] Hugo Vara,[4,†] Mario Dell'Agli,[1] Flamino Cattabeni,[1] Maurizio Giustetto,[4] Tiziana Borsello,[2] Gianluigi Forloni,[2] Alessandro Padovani[3] and Monica Di Luca[1]

1 Department of Pharmacological Sciences and Centre of Excellence on Neurodegenerative Diseases, Università degli Studi di Milano, 20133 Milan, Italy
2 Department of Neuroscience, Mario Negri Institute, 20156 Milan, Italy
3 Department of Neurological Sciences, University of Brescia, 25125 Brescia, Italy
4 Department of Anatomy, Pharmacology and Forensic Medicine, University of Turin and National Institute of Neuroscience – Italy, 10126 Turin, Italy

*These authors contributed equally to this work.
†Present address: Instituto de Neurociencias de Alicante, Universidad Miguel Hernández – CSIC. Sant Joan d'Alacant, 03550 Alicante, Spain.

Correspondence to: Monica Di Luca,
Università degli Studi di Milano,
Department of Pharmacological Sciences,
Via Balzaretti, 9;
20153 Milano, Italy
E-mail: monica.diluca@unimi.it

We describe here an innovative, non-transgenic animal model of Alzheimer's disease. This model mimics early stages of sporadic disease, which represents the vast majority of cases. The model was obtained by interfering with the complex between a disintegrin and metalloproteinase domain containing protein 10 (ADAM10), the main α-secretase candidate, and its partner, synapse-associated protein 97, a protein of the postsynaptic density-membrane associated guanylate kinase family. Association of ADAM10 with synapse-associated protein 97 governs enzyme trafficking and activity at synapses. Interfering with the ADAM10/synapse-associated protein 97 complex for 2 weeks by means of a cell-permeable peptide strategy is sufficient to shift the metabolism of the amyloid precursor protein towards amyloidogenesis and allows the reproduction of initial phases of sporadic Alzheimer's disease. After 2 weeks of treatment, we detected progressive Alzheimer's disease-like neuropathology, with an increase of β-amyloid aggregate production and of tau hyperphosphorylation, and a selective alteration of N-methyl-D-aspartic acid receptor subunit composition in the postsynaptic compartment of mouse brain. Behavioural and electrophysiological deficits were also induced by peptide treatment.

Keywords: animal models; SAP97; NMDA; synaptopathy; amyloid precursor protein metabolism

Abbreviations: ADAM10 = a disintegrin and metalloproteinase domain with protein 10; Aβ = β-amyloid peptide; Ala = Tat-Ala ADAM10$^{709-729}$ peptide; CTF = carboxy terminal fragment; Pro = Tat-Pro ADAM10$^{709-729}$ peptide; SAP97 = synapse-associated protein 97; TIF = Triton-X insoluble fraction

Received March 4, 2010. Revised May 25, 2010. Accepted June 20, 2010. Advance Access publication August 30, 2010

Introduction

Alzheimer's disease is the most common cause of dementia and no cure is available at the moment. The underlying neuropathology of Alzheimer's disease includes extracellular deposition of β-amyloid peptide (Aβ), intraneuronal accumulation of aberrant forms of hyperphosphorylated tau (Selkoe, 2001) as well as synapse dysfunction and neuronal loss (DeKosky and Scheff, 1990; Selkoe, 2002).

Substantial data indicate accumulation of Aβ in the brain, particularly in its non-fibrillar soluble oligomeric forms, as the primary influence driving Alzheimer's disease pathogenesis (Hardy and Higgins, 1992). The rest of the disease process, including formation of neurofibrillary tangles and synapse loss, is considered a downstream consequence of Aβ deposition and it is proposed to result from an imbalance between Aβ production and Aβ clearance. Aβ derives from the concerted action of β–secretase (Vassar *et al.*, 1999), which mediates amyloid precursor protein shedding at Aβ N-terminus and γ-secretase, responsible for amyloid precursor protein C-terminal stub cleavage (De Strooper *et al.*, 1998). Alternatively, amyloid precursor protein processing is exerted by a disintegrin and metalloproteinase (ADAM10) family member that prevents Aβ formation (Lammich *et al.*, 1999; Postina *et al.*, 2004).

The generation of animal models that recapitulate characteristic features of Alzheimer's disease is of great relevance to improve the understanding of disease pathogenesis and to develop new therapies. Current models of Alzheimer's disease rely on information gathered from inherited familiar forms. Identification in various human pedigrees of gene mutations in amyloid precursor protein (Goate *et al.*, 1991), in presenilin-1 and -2 (Scheuner *et al.*, 1996) provided a potential tool of generating rodent models of the disease. Despite their undoubted value, transgenic Alzheimer's disease mice show a number of pitfalls, i.e. they fail to model the progressive stages of the disease, which questions their role as pre-clinical models of Alzheimer's disease. There is no mouse line that models aetiology of late-onset/age-related sporadic Alzheimer's disease, which accounts for the vast majority of cases. Thus, focusing on new hypotheses concerning Alzheimer's disease pathogenesis and on the corresponding modelling is now a need.

Recently, Kim and colleagues reported two potentially pathogenic mutations with incomplete penetrance for late-onset familial Alzheimer's disease in the region encoding the prodomain sequence in the gene for ADAM10 (Kim *et al.*, 2009). ADAM10 interacts directly with synapse-associated protein (SAP) 97, a cargo protein of the postsynaptic density-membrane associated guanylate kinase (PSD-MAGUK) family (Marcello *et al.*, 2007). Since SAP97 is involved in the trafficking of molecules to the glutamatergic synapse (Leonard *et al.*, 1998; Sans *et al.*, 2001) and in events controlling synaptic transmission, its role in neurodegenerative diseases has been largely addressed and alterations have been identified in early stages of several disorders (Nash *et al.*, 2005; Lau and Zukin, 2007). The direct binding of proline-rich domains of the tail of ADAM10 to the SH3 domain of SAP97 promotes ADAM10 trafficking to synaptic membranes and regulates enzyme activity on amyloid precursor protein in primary neuronal cultures and, acutely, in rodent brains (Marcello *et al.*, 2007). Therefore, interfering with ADAM10/SAP97 complex appears as an ideal approach to investigate the connection between amyloid precursor protein metabolism and synaptic dysfunction in early phases of Alzheimer's disease.

Here, we describe the generation of an innovative mouse model of Alzheimer's disease through uncoupling of ADAM10 from SAP97. Disruption of the ADAM10/SAP97 complex is sufficient to reduce ADAM10 levels at synaptic sites as well as to decrease its activity, thus shifting amyloid precursor protein metabolism towards amyloidogenesis and reproducing the different events of sporadic Alzheimer's disease.

Material and methods

Ex vivo studies

Hippocampi from six patients with Alzheimer's disease and six healthy controls were obtained from The Netherland Brain Bank. Established Braak and Braak criteria were used to categorize Alzheimer's disease tissues (Braak and Braak, 1991). Healthy controls had no history of psychiatric or neurological disease and no evidence of age-related neurodegeneration. All procedures were in accordance with the National Institutes of Health Guide for Care and Use of laboratory human tissues and were approved by the Ethics Committee of the University of Milan.

Animal treatment

Adult male C57BL/6 mice, 8 weeks old, were treated with the cell-permeable peptide Tat-Pro ADAM10$^{709\text{-}729}$ (Pro, NH_2-YGRKKRR QRRRPKLPPPKPLPGTLKRRRPPQP-COOH), obtained by linking the 11 amino acid human immunodeficiency virus Tat transporter to a 21 amino acid sequence corresponding to the ADAM10 proline-rich domains, or with Tat-Ala ADAM10$^{709\text{-}729}$ (Ala, NH_2-YGRKKRRQRRRA KLAAAKALAGTLKRRRAAQA-COOH) (Xigenpharma, Lausanne, CH). Peptides were conjugated to fluorescein. Peptides were administered subcutaneously for 7 or 14 days through osmotic minipumps (Alzet2002, Charles River, Calco, LC, Italy) or injected intraperitoneally for 1 day. Dose regimens corresponded to 1 nmol/g. Animals were killed 1, 7 or 14 days after treatment and the brain was rapidly dissected. Four independent experiments with the two groups, Ala and Pro (three animals per group) were performed for biochemical experiments. Animal handling and surgical procedures were carried out with care taken to minimize discomfort and pain in accordance with ethical regulations and guidelines of the European Communities Council (Directive of 14 November 1986, 86/609/EEC).

Sample preparation

Triton-X insoluble fraction (TIF) and soluble fraction S2 were obtained as previously described (Gardoni *et al.*, 2001; Marcello *et al.*, 2007).

Sodium dodecyl sulphate polyacrylamide gel electrophoresis

Samples (homogenate and TIF) were separated by electrophoresis on a 7% sodium dodecyl sulphate polyacrylamide gel electrophoresis

(SDS–PAGE) gel, while the S2 fraction was separated on a 6% SDS–PAGE gel. To detect amyloid precursor protein carboxy terminal fragments (CTFs), Tris–Tricine gels at 15% were used. Proteins were transferred to a nitrocellulose membrane and probed with the corresponding primary antibody followed by incubation with appropriate horseradish peroxidase-conjugated secondary antibodies (Pierce, Rockford, IL, USA).

Immunohistochemistry

Mice were deeply anaesthetized with tribromoethanol (intraperitoneally, 1 mg/kg) and perfused through the ascending aorta with physiological saline followed by fixative solution (4% paraformaldehyde in 0.1 M phosphate buffer, pH 7.4). Brains were removed and post-fixed overnight at 4°C in the same fixative. Series of 50 μm thick coronal sections were cut using a vibratome. For Congo Red staining, slices were washed in water, incubated in 1% Congo Red solution and then differentiated in alkaline alcohol (0.2% KOH in 80% ethanol) and counterstained with haematoxylin. For tau phosphorylation immunostaining, sections were washed in phosphate-buffered saline, treated with 2% H_2O_2 in phosphate-buffered saline and incubated in 5% normal goat serum in phosphate-buffered saline containing 0.5% Triton X-100. Sections were incubated with anti-tau AT8 antibody at a concentration of 5 mg/ml, overnight at 4°C. Biotinylated goat-anti-mouse IgG (Vector, Burlingame, CA, USA) was applied at a dilution of 1:500, followed by incubation with streptavidin-conjugated horseradish peroxidase (Vector) for 1 h. Tissue-bound peroxidase was detected using 3,3-diamino-benzidine (0.025%) as a chromogen. Immunoreacted sections were placed on microscope slides and coverslipped with mounting medium.

Immunoprecipitation

Fifty μg of (for ADAM10/SAP97, Akap79/150/SAP97, GluR1/SAP97 and PYK-2/PSD-95 immunoprecipitation) or 70 μg (for SAP97/NR2A immunoprecipitation) of homogenate from mice treated with Ala or Pro were incubated overnight with an antibody against ADAM10, Akap79/150, GluR1, PYK2 or SAP97. Co-immunoprecipitation was carried out as previously described (Marcello *et al.*, 2007).

Determination of Aβ release

For evaluation of Aβ release from mice treated with Ala or Pro, an enzyme-linked immunosorbent assay kit was used (IBL, Gunma, Japan). The test was performed on total homogenate following the manufacturer's instructions. A standard curve ranging from 0 to 800 pg/ml was obtained with each point corresponding to the average of two measurements.

Quantification and statistical analysis

Quantification of western blot analysis was performed by computer-assisted imaging (Quantity-One® System, BioRad, Hercules, CA, USA) and statistical evaluations were performed according to two-tailed paired Student's *t*-test or one-way ANOVA followed by appropriate *post hoc* tests. Quantification of immunostaining is shown as fold difference compared with controls (healthy controls or Ala) in the same experiment. Values are means ± SEM for four independent experiments for a total of 24 animals.

Hippocampal slice preparation and electrophysiology

Fourteen days after surgical minipump insertion, mice were decapitated without anaesthesia. Hippocampi were quickly dissected out in ice-cold oxygenated artificial CSF containing the following (in mM): 120 NaCl, 2.5 KCl, 2.5 $CaCl_2$, 1.2 $MgCl_2$, 26.2 $NaHCO_3$, 1.0 NaH_2PO_4 and 11.0 glucose, bubbled with a mixture of 95% O_2/5% CO_2, pH 7.4. Transverse hippocampal slices (400 μm; $n = 8$ slices from $n = 3$ mice per group) were cut and maintained in a humidified holding chamber at room temperature for 1 h for recovery. Individual slices were transferred to an interface recording chamber (Fine Science Tools, Foster City, CA, USA) where they were continuously perfused with artificial CSF maintained at 29°C, at a flow rate of 1.5–2 ml/min. Extracellular field excitatory postsynaptic potentials were recorded in the stratum radiatum of area CA1 of the hippocampus using glass electrodes filled with 3 M NaCl coupled to the input stage of a Warner IE-210 amplifier (Handen, CT, USA). Stimuli were delivered to the commissural/Schaffer collateral afferents at 0.033 Hz (0.1 ms pulse duration) with a concentric bipolar stainless steel electrode. Data were collected and analysed online (10 kHz sampling rate) using pClamp software (Clampex, Axon Instruments, CA, USA). A stimulus intensity that elicited an extracellular field excitatory postsynaptic potential amplitude that was ~33% of the maximum was used. Long-term potentiation was induced by a high-frequency stimulation, consisting of four trains of 100 Hz for 1 s, separated by 30 s. Synaptic activity was measured as the maximal slope of the rising phase of the extracellular field excitatory postsynaptic potential. Each experiment was normalized to the mean value of the extracellular field excitatory postsynaptic potential slope recorded during the baseline (20 min of stable recording before high-frequency stimulation). Long-term potentiation values were calculated as the percentage increase in the extracellular field excitatory postsynaptic potential slope 50–60 min after the end of high-frequency stimulation compared with the baseline value. Data are presented as means ± SEM, and ANOVA was used for statistical analysis.

Novel object recognition

Twelve days after surgical minipump insertion, mice treated with Ala and Pro ($n = 9$ per group) were habituated to the test arena for 5 min in the absence of any object. In the first trial, the mice were presented for 10 min with two objects of identical size and shape. In the second trial, the mice were presented for 10 min with a duplicate of one of the objects from the first trial and a new object differing in shape. During both trials, exploration of the object was defined as the time spent sniffing, licking or touching the object. The discrimination index [novel (t) − familiar (t)]/[total time (t) at novel + familiar], number of total movements in 5 min and time (s) spent investigating in 10 min were evaluated. Results are shown as mean ± SEM, and ANOVA followed by Fisher as a *post hoc* test were used for statistical analysis.

DyOlistic labelling

Fourteen days after surgical minipump insertion, mice treated with cell-permeable peptides Pro and Ala ($n = 6$ per group) were anaesthetized and perfused with paraformaldehyde. Transverse hippocampal CA1 apical and cortical layer I slices (300 μm) were cut with a vibratome and slices were kept in phosphate buffer. Tungsten particles were coated with a lipophilic dye, DiI (Molecular Probes, Eugene, OR, USA). Microcarriers were loaded into the gene gun and then

fired into tissue slices with the BioRad Gene Gun with a gas pressure 200 psi at a distance of 40 mm. Slices were kept for 10 min in 0.1 M phosphate buffer and then for 2 h in 4% paraformaldehyde. After 24 h, images of DiI-labelled structures in hippocampal CA1 stratum radiatum and layer I of the somatosensory cortex were acquired using the Zeiss Confocal LSM510 microscope with ×63 objective. At least 10 *z*-stack images were acquired for each animal and for each area of interest. The ImageJ software program was used to quantify DiI-labelled neurons. Dendritic segments were chosen randomly and were at least one soma's length away from the cell soma. Four parameters were measured, including spine density, spine area, spine length and spine head diameter. All measurements were made with the investigator blinded to the treatment used. Results are shown as means of $n = 33$ neurons ± SEM (at least 10 spines were measured for each neuron) and Student's *t*-test was used for statistical analysis.

Antibodies

The following antibodies were used: polyclonal antibody anti-ADAM10 and polyclonal antibody AB2072 against amyloid precursor protein from Abcam (Cambridge, MA, USA); monoclonal antibody anti-GluR1, monoclonal antibody anti-PYK-2 and monoclonal antibody anti-α-CaMKII from Millipore (Billerica, MA, USA); monoclonal antibody anti-SAP97 from Stressgen (Ann Arbor, MI, USA). Polyclonal antibody anti-Actin, monoclonal antibody anti-Tubulin and monoclonal antibody anti-NR2A from Sigma (St Louis, MO, USA); monoclonal antibody AT8 against tau from Pierce; monoclonal antibody anti-GluR2 and monoclonal antibody anti-PSD-95 from Neuromab (Davis, CA, USA); monoclonal antibody anti-NR1 and polyclonal antibody anti-NR2B from Invitrogen (Carlsbad, CA, USA); polyclonal antibody anti-AKAP79/150 from Santa Cruz Biotechology (Santa Cruz, CA, USA); and monoclonal antibody anti-*N*-Cadherin from BD Bioscience (Sparks, MD, USA).

Results

ADAM10/SAP97 association is reduced in mice after 2 weeks of treatment with Pro peptide and in Alzheimer's disease patients at Braak level 4

Interfering acutely with the ADAM10/SAP97 complex inhibits ADAM10 trafficking to the postsynaptic membrane and its activity in rodents (Marcello *et al.*, 2007).

On the basis of this observation, we supposed that subchronic disruption of the ADAM10/SAP97 complex could mimic one of the events occurring in sporadic Alzheimer's disease and could allow the generation of a model of Alzheimer's disease.

To investigate this, Tat-Pro ADAM10$^{709–729}$ peptide (Pro) (Marcello *et al.*, 2007) was used, in which ADAM10 proline-rich domains (amino acids 709–729), responsible for binding to SAP97, are fused to the Tat transporter sequence (Aarts *et al.*, 2002; Fig. 1A). Eight-week-old mice were exposed subcutaneously for 2 weeks to the Pro peptide. As a control, we used an inactive peptide, Tat-Ala ADAM10$^{709-729}$ (Ala), where all prolines were substituted by alanines.

To validate our tool, peptide penetration into neurons was confirmed by double staining with an anti-Tat antibody, used to visualize peptides, and an anti-MAP-2 antibody, used as a neuronal marker (Supplementary Fig. 1). Peptide capability to interfere with the association between SAP97 and ADAM10 was investigated by co-immunoprecipitation experiments from total brain homogenates. A reduction of the ADAM10/SAP97 immunocomplex was observed in mice treated with Pro compared with Ala (Fig. 1B; $n = 4$, $P = 0.005$, $-41.3 \pm 6.5\%$, Pro versus Ala). We found no modifications of SAP97 and ADAM10 levels in total homogenate, suggesting that the observed uncoupling can be ascribed to a decreased association rather than to changes in levels of these proteins (Fig. 1C; ADAM10: $n = 4$; $P > 0.05$; $+12.6 \pm 4.9\%$; SAP97: $n = 4$; $P > 0.05$; $+9.7 \pm 10.7\%$, Pro versus Ala).

To validate the relevance of the ADAM10/SAP97 complex for Alzheimer's disease pathogenesis, we performed a biochemical analysis of hippocampi from Alzheimer's disease patients at Braak level 4 (Braak and Braak, 1991) and of age-matched healthy controls. Braak level 4 corresponds to initial stages of sporadic disease, and the hippocampus was analysed as a strongly affected area. Total brain homogenates from hippocampi of healthy controls and patients with Alzheimer's disease were immunoprecipitated with anti-ADAM10 antibody, and SAP97 co-immunoprecipitation was evaluated. We revealed a decrease of the ADAM10/SAP97 immunocomplex in Alzheimer's disease patients compared with healthy controls (Fig. 1D; $n = 6$; $P = 0.001$, $-33.7 \pm 4.9\%$, Alzheimer's disease versus healthy controls), suggesting uncoupling of the ADAM10/SAP97 complex as an early event in Alzheimer's disease pathogenesis. No differences were detected between healthy controls and patients with Alzheimer's disease in SAP97 and ADAM10 levels in total brain homogenates (SAP97: $n = 6$, $P > 0.05$; $+31.4 \pm 35.1\%$; ADAM10: $n = 6$, $P > 0.05$, $-7.7 \pm 11.7\%$, Alzheimer's disease versus healthy controls), underlying that the ADAM10/SAP97 complex is not reduced in Alzheimer's disease due to lower expression of the two proteins.

Pro peptide is specific in disrupting ADAM10/SAP97 complex

We investigated Pro peptide specificity in disrupting the ADAM10/SAP97 complex, without influencing other protein–protein interactions.

First, the capability of SAP97 SH3 domain to bind other partners in the presence of Pro was evaluated. Cell-based studies suggest that Akap79/150, a signalling scaffold, is recruited to AMPA (α-amino-3-hydroxy-5-methyl-4-isoxazole-propionic acid) receptors through interaction with SH3/GK domains of SAP97 (Colledge *et al.*, 2000). We performed co-immunoprecipitation experiments between SAP97 and Akap79/150. No alterations were found in Akap79/150/SAP97 association (Fig. 2A; $n = 4$, $P > 0.05$, $-8.7 \pm 31.3\%$, Pro versus Ala). SAP97 has been recognized as a cargo element responsible for synaptic trafficking of key elements of the glutamatergic synapse, i.e. the NR2A subunit of the glutamate *N*-methyl-D-aspartic acid (NMDA) receptor (Gardoni *et al.*, 2003) and the GluR1 subunit of the glutamate

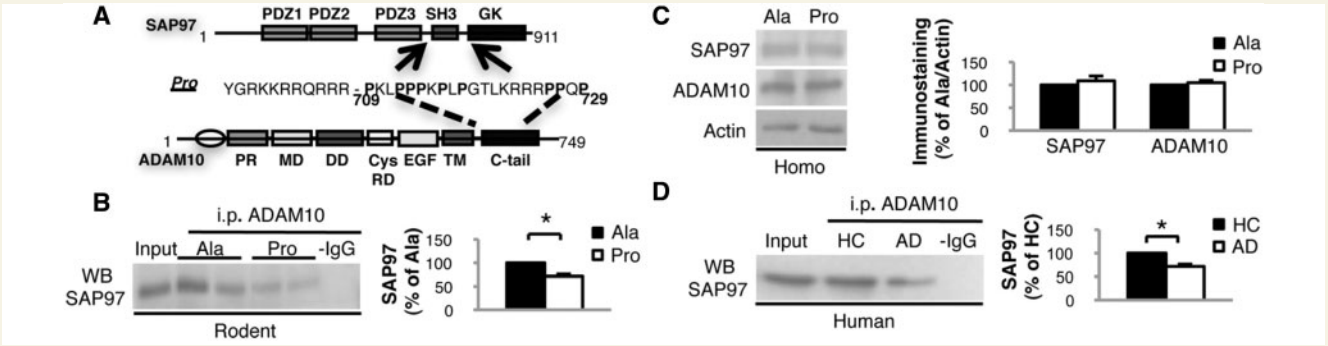

Figure 1 ADAM10/SAP97 association is reduced after 2 weeks of treatment with Pro peptide and in patients with Alzheimer's disease. (**A**) Schematic representation of SAP97, ADAM10 and Pro peptide. (**B**) C57BL/6 mice were treated for 2 weeks with Pro or Ala peptides and total brain homogenates were co-immunoprecipitated with anti-ADAM10 antibody. SAP97 presence was evaluated in the immunocomplex. Treatment with Pro peptide decreases the association of the two proteins ($P = 0.005$). (**C**) Western blot of homogenate from Pro- and Ala-treated mice performed with anti-ADAM10 and anti-SAP97 antibodies. No changes were detectable in ADAM10 and SAP97 levels. All data were normalized to actin. (**D**) Homogenate from hippocampi of healthy controls (HC) and patients with Alzheimer's disease (AD) was immunoprecipitated with anti-ADAM10 antibody and SAP97 co-precipitation was evaluated. ADAM10/SAP97 association is reduced in Alzheimer's disease patients compared with healthy controls ($P = 0.001$). For all experiments, quantitative analysis of immunostaining is shown as percentage of control (Ala or healthy controls) in the same experiment. i.p. = immunoprecipitation; WB = western blot.

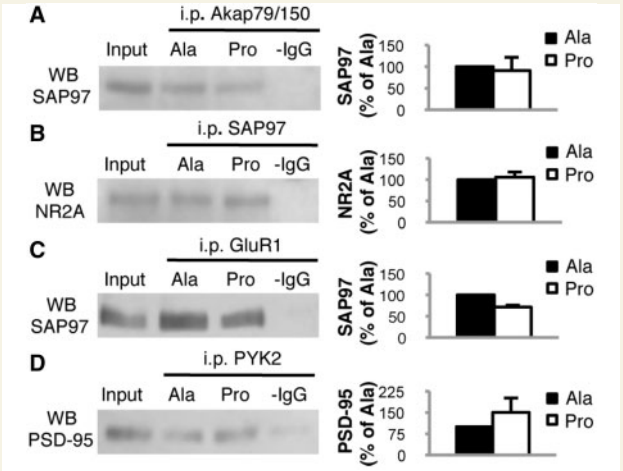

Figure 2 Pro peptide treatment does not interfere with protein–protein complexes other than ADAM10/SAP97. (**A**) C57BL/6 mice were treated for 2 weeks with Pro or Ala peptides and total brain homogenates were co-immunoprecipitated with anti-Akap79/150 antibody. SAP97 presence was evaluated in the immunocomplex. The association is not altered by treatment. (**B**) C57BL/6 mice were treated for 2 weeks with Pro or Ala peptides and total brain homogenates were co-immunoprecipitated with anti-SAP97 antibody. NR2A presence was evaluated in the immunocomplex. The association is not altered by treatment. (**C**) C57BL/6 mice were treated for 2 weeks with Pro or Ala peptides and total brain homogenates were co-immunoprecipitated with anti-GluR1 antibody. SAP97 presence was evaluated in the immunocomplex. The association is not altered by treatment. (**D**) C57BL/6 mice were treated for 2 weeks with Pro or Ala peptides and total brain homogenates were co-immunoprecipitated with anti-PYK2 antibody. PSD-95 presence was evaluated in the immunocomplex. The association is not altered by treatment. For all experiments, quantitative analysis of immunostaining is shown as percentage of Ala treatment in the same experiment. i.p. = immunoprecipitation; WB = western blot.

AMPA receptor (Sans *et al.*, 2001). Pro specificity was assessed by analysing the binding of these partners to SAP97 by co-immunoprecipitation between SAP97 and NR2A, as well as between SAP97 and GluR1. No alterations were found in either SAP97/NR2A association (Fig. 2B; $n = 4$, $P > 0.05$, $+6.3 \pm 20.4\%$, Pro versus Ala) or in the SAP97/GluR1 immunocomplex (Fig. 2C; $n = 4$, $P > 0.05$, -21.2 ± 9.4, Pro versus Ala) after treatment. Moreover, the Pro peptide did not interfere with binding of other synaptic SH3 to Pro-rich domains, as assessed by co-immunoprecipitation of PYK2 and PSD-95 (Fig. 2D; $n = 4$; $P > 0.05$, $+50.4 \pm 51.2$, Pro versus Ala; Seabold *et al.*, 2003). Altogether, these data indicate that Pro is specific for its capability to interfere with the ADAM10/SAP97 complex.

Treatment with Pro alters ADAM10 localization and generates the characteristic features of Alzheimer's disease: amyloidogenesis and tau hyperphosphorylation

SAP97 is necessary to drive ADAM10 to the plasma membrane (Marcello *et al.*, 2007). We asked whether the reduction in ADAM10/SAP97 association, obtained through Pro peptide treatment, could induce a modification in ADAM10 localization. Western blot analysis performed on TIF—a fraction enriched in proteins of the postsynaptic density (Gardoni *et al.*, 2001)—revealed a statistically significant reduction of ADAM10 levels in mice treated with Pro compared with mice treated with Ala (Fig. 3A; $n = 4$; $P = 0.006$, $-16.7 \pm 2.2\%$, Pro versus Ala). No changes were observed in SAP97 immunoreactivity in the TIF (Fig. 3A; $n = 4$, $P > 0.05$, $-10.4 \pm 5.1\%$, Pro versus Ala).

Since ADAM10 is active at the plasma membrane (Lammich *et al.*, 1999), we supposed that the reduction of ADAM10 in the postsynaptic compartment could be paralleled by a decrease

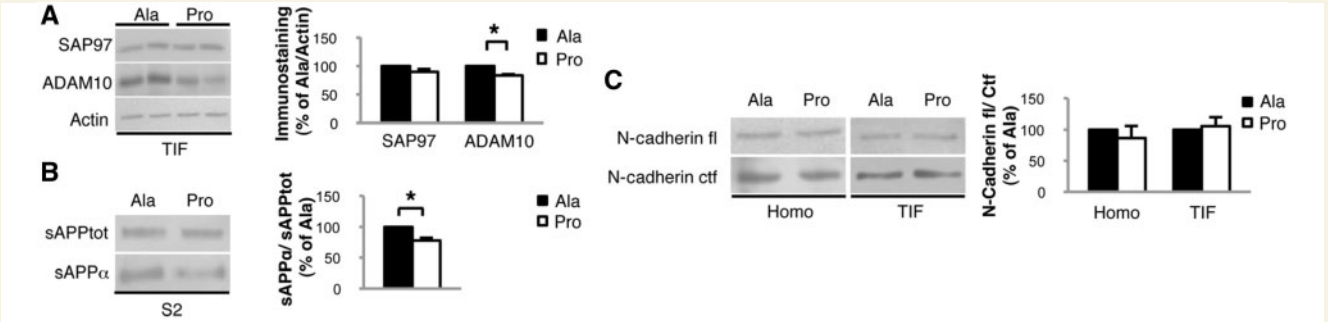

Figure 3 Pro treatment alters ADAM10 localization and activity on amyloid precursor protein. (**A**) Western blot of TIF from Pro- and Ala-treated mice performed with anti-ADAM10 and anti-SAP97 antibodies. Pro treatment reduced ADAM10 levels ($P = 0.006$) without modifying SAP97 levels. All data were normalized to actin. (**B**) Western blot performed on the soluble fraction S2 of mice treated with Pro or Ala peptides. sAPPα/sAPPtot ratio is reduced in mice treated with Pro peptide ($P = 0.043$). (**C**) Western blot performed on total brain homogenate and TIF fraction of Pro- and Ala-treated mice to reveal *N*-cadherin full-length (fl) and C-terminal fragment (Ctf). *N*-cadherin fl/Ctf ratio was not altered by the treatment with Pro peptide. For all experiments, quantitative analysis of immunostaining is shown as percentage of Ala treatment in the same experiment.

in its activity towards its synaptic substrates. sAPPα release, deriving from ADAM10 cleavage on amyloid precursor protein, was decreased in Pro-treated compared with Ala-treated mice (Fig. 3B; $n = 4$, $P = 0.043$, $-22.7 \pm 4.6\%$, Pro versus Ala), whereas we observed no alterations in the processing of *N*-cadherin, another ADAM10 synaptic substrate (Reiss *et al.*, 2005; Fig. 3C; $n = 4$; homogenate: $-9.1 \pm 19.6\%$; TIF: $+5.7 \pm 10.5\%$; overall $P > 0.05$, Pro versus Ala).

To exclude compensatory upregulation of other metalloproteases after 2 weeks of treatment, levels of matrix metallopeptidase 9 (MMP-9) and its gelatinolytic activity were analysed. No alterations were found in MMP-9 total brain homogenate levels or in its gelatinolytic activity (Supplementary Fig. 2A; $n = 4$; homogenate: $+12.2 \pm 5.6\%$, $P > 0.05$; Supplementary Fig. 2B; $n = 4$; zymography: $-8.7 \pm 6.5\%$, $P > 0.05$; Pro versus Ala).

Altered amyloid precursor protein metabolism induced by Pro peptide treatment was further investigated. We measured amyloid precursor protein CTFs: CTF83 for α-secretase and CTF99 for β-secretase cleavage, in TIF. The CTF83/CTF99 ratio was reduced in mice treated with Pro compared with mice treated with Ala, indicating a shift of amyloid precursor protein metabolism towards amyloidogenesis in Pro-treated mice (Fig. 4A; $n = 4$, $P = 0.03$, $-28.6 \pm 5.7\%$, Pro versus Ala). The shift of amyloid precursor protein metabolism towards Aβ production was further confirmed by the raise in $A\beta_{1-42}$ production detected by ELISA in total brain homogenate of mice treated with Pro if compared with Ala-treated mice (Fig. 4B, $n = 4$; $P = 0.02$; $+16.8 \pm 4.6\%$, Pro versus Ala).

An initiating factor in Alzheimer's disease pathogenesis occurs when soluble, monomeric Aβ undergoes a conformational change and converts into oligomeric forms (Klein *et al.*, 2001). Although murine Aβ is less prone to aggregation than human Aβ, we detected low-*n* Aβ oligomers in formic acid soluble extracts obtained by sequential centrifugation of brain homogenates (Lesne *et al.*, 2006). An antibody raised against the N-terminus of Aβ, AB2072, revealed an increase of an oligomeric aggregate at 16 kDa, a molecular mass corresponding to tetramers (Fig. 4C; $n = 4$, $P = 0.0005$, $+18.3 \pm 1.8\%$, Pro versus Ala) in Pro-treated mice. The detection of this band with AB2072 and 4G8, recognizing Aβ mid-domain, excludes the possibility that it represents degradation products of soluble amyloid precursor protein. The band was not recognized by antibodies for epitopes at the C-terminus or the N-terminus of amyloid precursor protein, amyloid precursor protein C-Term and 22C11, respectively, indicating it was neither one of the amyloid precursor protein CTFs nor amyloid precursor protein cleavage-end products (Supplementary Fig. 3A and Supplementary Methods). As revealed by Congo Red staining, we detected no plaques in Pro- and Ala-treated mice (Fig. 4D), suggesting that we are mimicking the early stages of Alzheimer's disease (Oddo *et al.*, 2003).

Since Aβ production triggers the development of other Alzheimer's disease hallmarks, such as neurofibrillary tangles (Oddo *et al.*, 2003), we evaluated the presence of tau hyperphosphorylation. Tau phosphorylation in serine$^{202-205}$ was increased in mice treated with Pro peptide (Fig. 4E; $n = 4$, $P = 0.038$, $+53.2 \pm 15.0\%$, Pro versus Ala). This was corroborated by immunohistochemical analysis showing tau hyperphosphorylation in soma, axons and dendrites of neurons in the cerebral cortex of Pro-treated mice compared with Ala-treated ones (Fig. 4F). Tau-C3 antibody is specific for tau cleaved at aspartic acid^{421}, which represents a further stage of neurofibrillary tangle evolution in Alzheimer's disease (Gamblin *et al.*, 2003). Tau-C3 staining revealed no signal in both groups (Supplementary Fig. 3B).

Effects of Pro peptide treatment on spine morphology and on molecular composition of the excitatory glutamatergic synapse

Synaptic dysfunction appears as an early event in disease pathogenesis with synapse loss evident in patients at early stages of Alzheimer's disease and with mild cognitive impairment

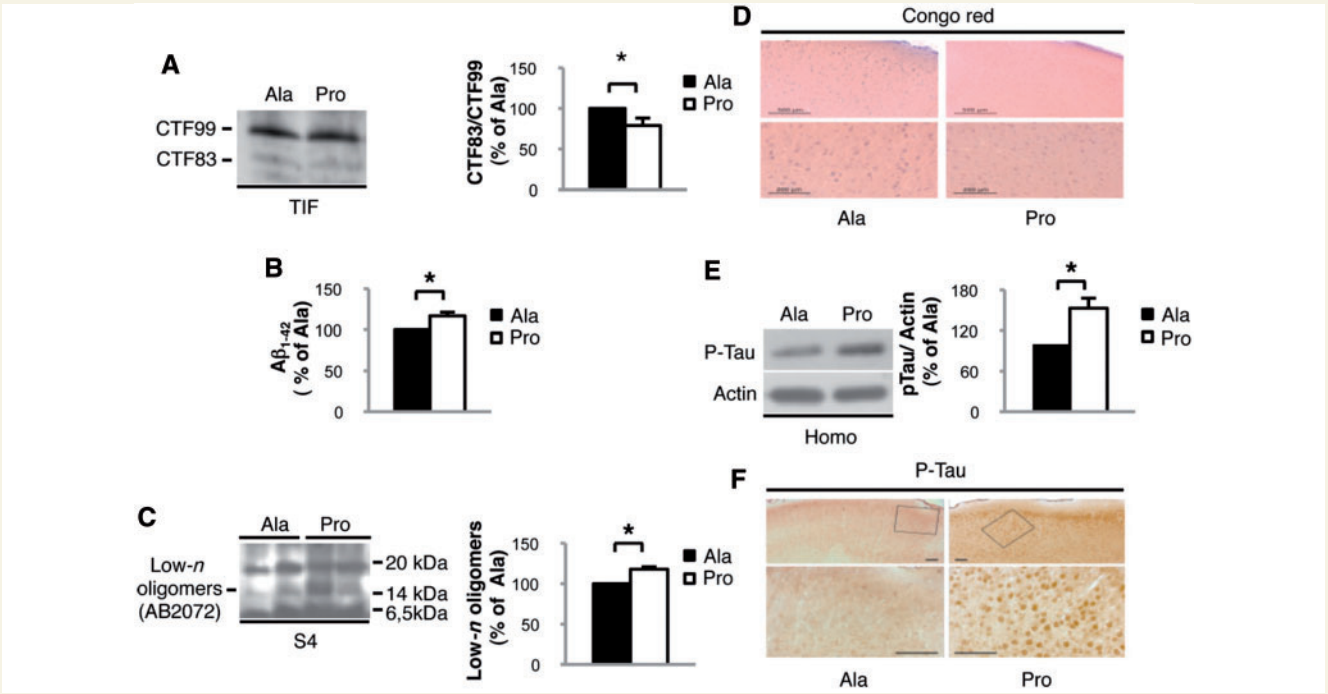

Figure 4 Pro treatment induces Alzheimer's pathological hallmarks. (**A**) Western blot performed on the TIF of Pro- and Ala-treated mice to reveal amyloid precursor protein CTFs. CTF83/CTF99 ratio is decreased in mice treated with Pro peptide ($P = 0.03$). (**B**) Quantification of $A\beta_{1\text{-}42}$ production in mice treated with Pro compared with Ala. $A\beta_{1\text{-}42}$ production is increased after Pro treatment ($P = 0.02$). (**C**) Western blot performed on the formic acid soluble fraction S4 of Pro- and Ala-treated mice to reveal Aβ oligomers. A 16 kDa band (at theoretical apparent molecular mass of tetramers) is increased after Pro treatment ($P = 0.0005$). (**D**) Representative images of Congo Red staining showing no senile plaques in Pro- and Ala-treated mice (scale bar = 500 μm and 200 μm). (**E**) Western blot performed on homogenate from mice treated with Pro or Ala peptides. Tau phosphorylation is increased in Pro-treated mice ($P = 0.038$). Data were normalized to actin. (**F**) Representative images of phosphorylated-tau (P-Tau) staining showing increased phosphorylation in Pro-treated mice (scale bar = 100 μm). For all experiments, quantitative analysis of immunostaining is shown as percentage of Ala treatment in the same experiment.

(Scheff *et al.*, 2007). We evaluated potential alterations of synaptic morphology associated with the observed shift of amyloid precursor protein metabolism towards amyloidogenesis. Analysis of dendritic spines was performed using DyOlistic fluorescent labelling (Gan *et al.*, 2000). We measured density (*N*/10 μm), area, neck length and head width of dendritic spines in the hippocampus and cortex. Statistical analysis showed no differences in all parameters between animals treated with Pro and Ala peptides, indicating that we are analysing the early stages preceding spine loss and degeneration [Fig. 5A; (i) cortex Ala: $n = 33$, area $0.384 \pm 0.009\ \mu m^2$, length 1.29 ± 0.02 μm, width 0.53 ± 0.01 μm, spines/10 μm 10.67 ± 0.42; Pro: $n = 33$, area $0.348 \pm 0.01\ \mu m^2$, length 1.30 ± 0.01 μm, width 0.557 ± 0.01 μm, spines/10 μm 10.53 ± 0.44; overall $P > 0.05$; Fig. 5B; (ii) hippocampus Ala: $n = 33$; area $0.312 \pm 0.009\ \mu m^2$, length 0.884 ± 0.01 μm, width 0.483 ± 0.008 μm, spines/10 μm 12.31 ± 0.573; Pro: $n = 33$, area $0.307 \pm 0.008\ \mu m^2$, length 0.84 ± 0.01 μm, width 0.474 ± 0.007 μm, spines/10 μm 12.10 ± 0.48; overall $P > 0.05$].

To characterize molecular events occurring prior to synaptic loss, we evaluated biochemically the composition of glutamatergic postsynaptic density. No alterations in PSD-95 (Fig. 6A; $n = 4$; homogenate: $+12.7 \pm 6.1\%$; TIF: $+1.2 \pm 6.6\%$; overall $P > 0.05$, Pro versus Ala) and α-CaMKII (Fig. 6A; $n = 4$; homogenate: $-1.1 \pm 2.7\%$; TIF: $+30.2 \pm 18.9\%$; overall $P > 0.05$, Pro versus Ala) levels were found, confirming no major modifications of postsynaptic density organization in early stages of Aβ formation. We detected no significant alterations in GluR1 (Fig. 6A; $n = 4$; homogenate: $+18.6 \pm 26.0\%$; TIF: $+20.3 \pm 23.1\%$; overall $P > 0.05$, Pro versus Ala) and GluR2 (Fig. 6A; $n = 4$; homogenate: $+0.9 \pm 10.9\%$; TIF: $+25.3 \pm 7.2\%$; overall $P > 0.05$, Pro versus Ala) AMPA receptor subunit levels in total homogenate and TIF in Pro-treated animals compared with Ala-treated ones. NR1, the NMDA receptor constitutive subunit, was unaltered (Fig. 6B; $n = 4$; homogenate: $+19.4 \pm 14.7\%$; TIF: $+20.2 \pm 8.0\%$; overall $P > 0.05$, Pro versus Ala) as was NR2B (Fig. 6B; $n = 4$; homogenate: $-2.6 \pm 5.4\%$; TIF: $+7.4 \pm 7.8\%$; overall $P > 0.05$, Pro versus Ala), but a specific reduction of NR2A subunit in TIF was observed (Fig. 6B; $n = 4$; homogenate: $+17.1 \pm 8.4\%$, $P > 0.05$; TIF: $-27.4 \pm 2.8\%$, $P = 0.002$, Pro versus Ala).

This modification of the molecular composition of glutamatergic postsynaptic density in Pro-treated mice temporally follows Aβ production. We evaluated the ADAM10/SAP97 immunocomplex (1 day: $P = 0.008$, $-32.4 \pm 3.9\%$; 7 days: $P = 0.003$, $-25.4 \pm 2.4\%$, Pro versus Ala), ADAM10 in TIF (1 day: $P = 0.04$, $-21.3 \pm 2.7\%$; 7 days: $P = 0.019$, $-17.5 \pm 4.2\%$, Pro versus Ala) as well as amyloid precursor protein metabolites at Days 1 and 7

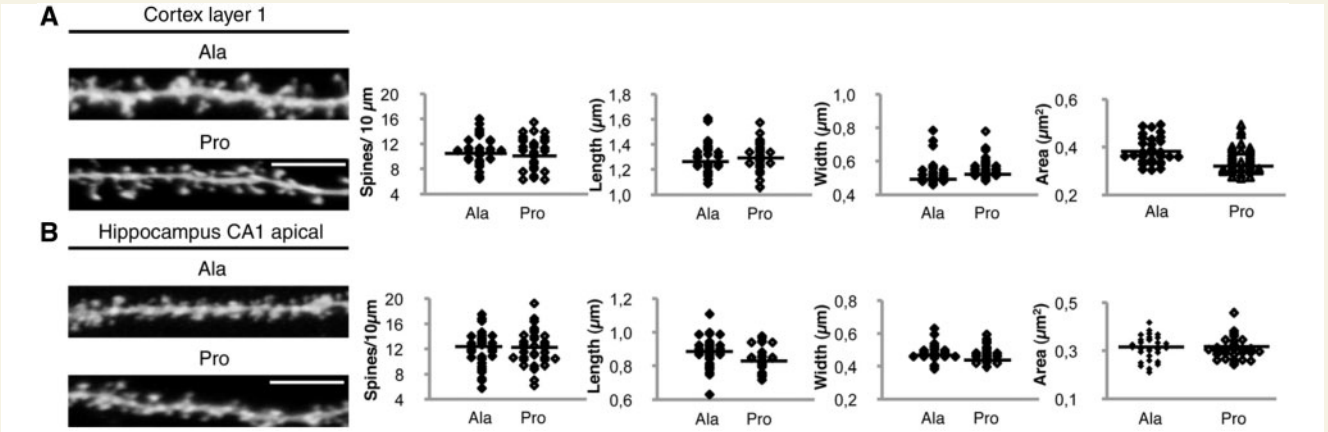

Figure 5 Effects of Pro treatment on spine density and morphology. Representative images of cortical layer I (**A**) and hippocampal CA1 apical (**B**) spines from Pro- and Ala-treated mice. Statistical analysis of spine density, neck length, head width and area revealed no modifications in both areas (scale bar = 5 μm).

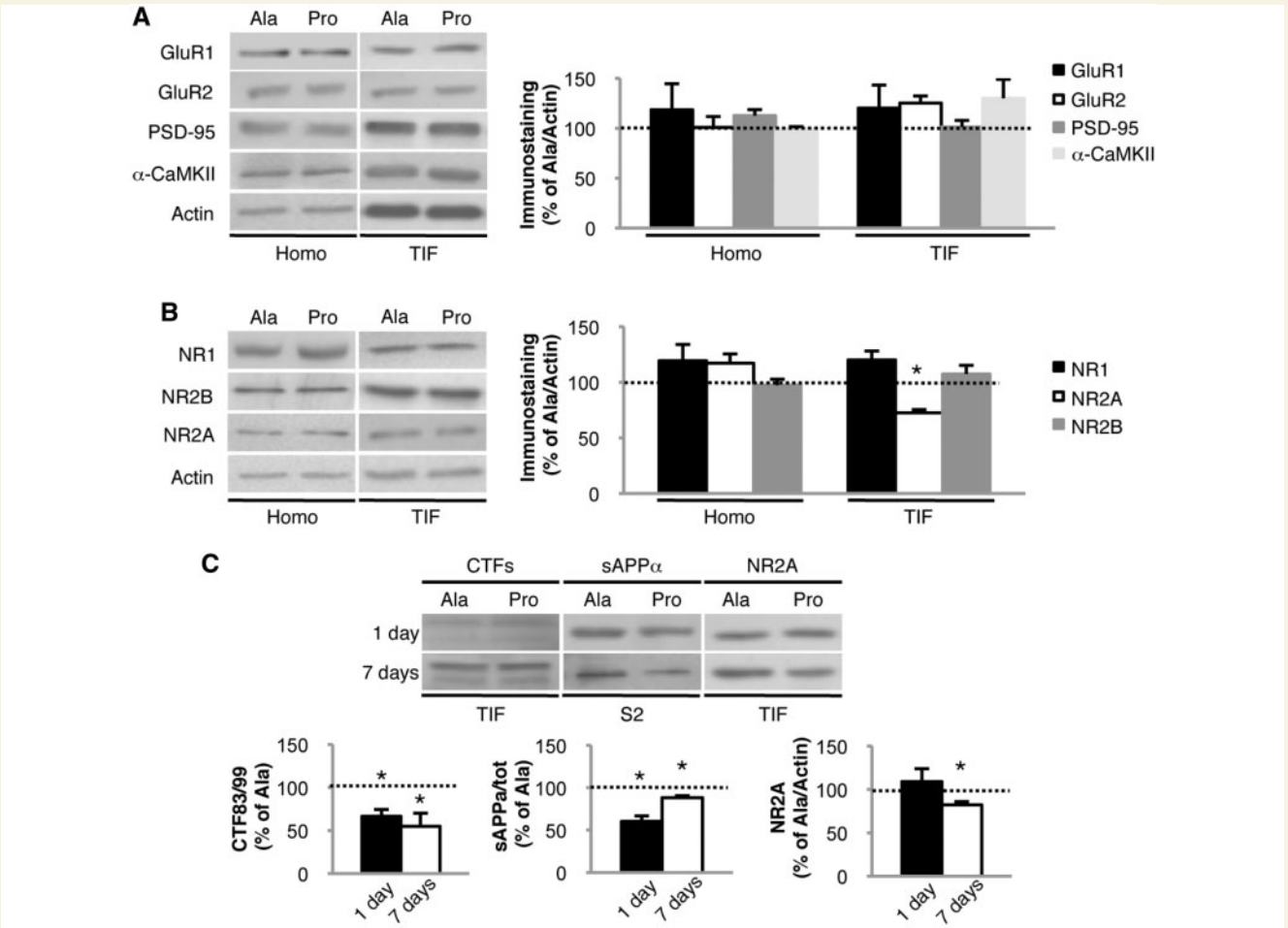

Figure 6 Effects of Pro treatment on the glutamatergic synapse. (**A**) Western blot of homogenate (Homo) and TIF from Pro- and Ala-treated mice performed with anti-GluR1, anti-GluR2, anti-PSD-95 and anti-α-CaMKII antibodies. (**B**) Western blot of homogenate and TIF from Pro- and Ala-treated mice performed with anti-NR1, anti-NR2A and anti-NR2B antibodies. NR2A is decreased in the TIF ($P = 0.002$). (**C**) Western blot analysis of the TIF and soluble fraction S2 of mice treated for 1 or 7 days with Pro or Ala. The CTF83/CTF99 ratio is reduced in mice treated with Pro peptide for 1 day ($P = 0.01$) and 7 days ($P = 0.035$). sAPPα/sAPPtot ratio is reduced in mice treated with Pro peptide for 1 day ($P = 0.02$) and 7 days ($P = 0.015$). NR2A is reduced in the TIF after 7 days of treatment with Pro ($P = 0.01$) but not after 1 day. All data were normalized to actin. For all experiments, quantitative analysis of immunostaining is shown as percentage of Ala treatment in the same experiment.

of treatment. sAPPα/total sAPP and CTF83/CTF99 ratios were shifted towards amyloidogenesis after both 1 and 7 days of treatment with the Pro peptide (Fig. 6C; 1 day: $n=4$; sAPPalpha/tot: $P=0.02$, $-39.7\pm5.2\%$; CTF83/99: $P=0.01$, $-34.3\pm7.9\%$, Pro versus Ala; 7 days: $n=4$; sAPPalpha/tot: $P=0.015$, $-10.1\pm2.3\%$; CTF83/99: $P=0.035$, $-45.8\pm15.2\%$, Pro versus Ala). In parallel, NR2A levels in TIF were measured. After 7 days, but not 1 day, of Pro peptide treatment, NR2A decreased in postsynaptic density (Fig. 6C; $n=4$, 1 day: $P>0.05$, $+9.1\pm14.8\%$; 7 days: $P=0.01$, $-17.8\pm3.5\%$, Pro versus Ala).

These results suggest that increases in Aβ production precede alterations of excitatory synapses.

Functional deficits: electrophysiological and behavioural consequences of Pro peptide treatment

We then evaluated activity-dependent synaptic plasticity. We tested long-term potentiation in the CA1 region of acute hippocampal slices obtained from mice treated with either the Pro or Ala peptide for 14 days. When potentiation of CA3–CA1 synapses was induced by high-frequency stimulation, no effects of peptide treatment were found on the magnitude of long-term potentiation measured 50–60 min after high-frequency stimulation. However, the maximum potentiation of the synaptic response immediately following high-frequency stimulation was significantly reduced in Pro-treated mice (Fig. 7A; $P<0.02$, ANOVA, Pro: $278.8\pm37.89\%$; Ala: $418.70\pm29.27\%$). This reduction of synaptic plasticity induced by the Pro peptide was statistically significant up to 10 min after high-frequency stimulation, a period in which enhancements of synaptic responses can be attributable to the buildup and decay of post-tetanic potentiation (Zucker and Regehr, 2002), a form of short-term synaptic plasticity.

To assess behavioural dysfunctions paralleling the alterations in synaptic organization and function, we performed a Novel Object Recognition test on animals treated with Pro or Ala for 2 weeks. Treated mice were unable to distinguish new objects from known ones, with no significant difference in the percentage of time spent investigating the two objects. Discrimination index between novel and familiar objects revealed a prominent effect of treatment with the Pro peptide. *Post hoc* analysis found a significant inability to discriminate between the two objects in Pro-treated mice [Fig.7B; discrimination index, Ala: 0.26; Pro: −0.01; saline: 0.3; ANOVA (Pro/Ala) $P=0.04$]. To assess whether administration of the peptides influenced the mobility of mice, the number of total movements in 5 min was determined and no significant differences were found between the groups [Fig. 7C; number of movements/5 min, Ala: 139.8 ± 8.5; Pro: 156.6 ± 13.7; saline: 157.8 ± 14.0; ANOVA (Pro/Ala) $P>0.05$].

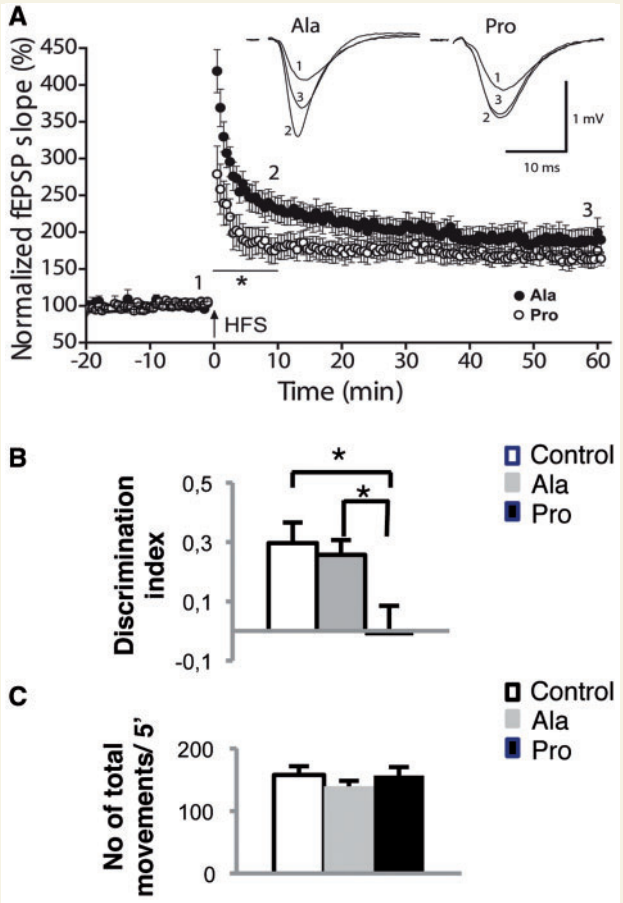

Figure 7 Effects of Pro-treatment on glutamatergic synapse function. (**A**) A reduction in post-tetanic potentiation induced by high-frequency stimulation (HFS; 4×100 Hz, 1 s, 30 s apart) was observed in Pro-treated mice (open circles, $n=8$ slices from $n=3$ mice) compared with Ala-treated (full circles, $n=8$ slices from $n=3$ mice; $P<0.01$, ANOVA). Long-term potentiation measured 50–60 min after HFS was similar in the presence of either peptide. Insets illustrating averaged extracellular field excitatory postsynaptic potentials from three consecutive traces taken before (1) and at different times after HFS (2 and 3) are shown above summary data. Error bars indicate SEM. (**B**) Quantification of the discrimination index of mice treated with Pro or Ala peptides in the novel object recognition test. Mice treated with Pro peptide show a reduced discrimination index compared with those treated with Ala peptide ($P=0.042$, ANOVA) and with saline-treated mice ($P=0.021$, ANOVA). (**C**) Quantification of the number of movements in 5 min in mice treated with Pro or Ala peptides in the Novel Object Recognition test. All behavioural data are expressed as means ± SEM ($n=9$ per group).

Discussion

Development of adequate animal models mimicking all stages of Alzheimer's disease progression and merging convergent pathways of pathogenesis still represents a need for research on Alzheimer's disease. Available mouse models have been generated on the basis of identified human mutations (Goate *et al.*, 1991; Scheuner *et al.*, 1996). Although informative for the understanding of molecular pathogenesis of the disease, these models present a number of weaknesses (Epis *et al.*, 2010; Morrissette *et al.*, 2009). In transgenic models, mutated proteins are chronically overexpressed and exposure to Aβ overproduction starts before

the common clinical onset of Alzheimer's disease. The genetic strains, the mutations and the different transcriptional promoters used to drive their expression, as well as other factors that are not completely known, produce different amounts of Aβ, forming potentially different oligomeric forms, which may induce high variability and different outcomes across transgenic mouse models (Epis *et al.*, 2010; Gerlai, 1996; Morrissette *et al.*, 2009).

Here, we propose a different approach to investigating the consequences of Aβ increase in an innovative, non-transgenic animal model of early Alzheimer's disease.

Our strategy is based on interference with the ADAM10/SAP97 protein complex in adult mice. We have already reported the interaction with the PSD-MAGUK protein SAP97 as pivotal for ADAM10 trafficking to the postsynaptic membrane and for its enzymatic non-amyloidogenic cleavage on amyloid precursor protein (Marcello *et al.*, 2007). The relevance of the ADAM10/SAP97 complex in early stages of disease is strengthened by our analysis of the hippocampus of patients at Braak level 4 of Alzheimer's disease, where we observed a clear reduction in ADAM10/SAP97 co-immunoprecipitation. These results suggest that the defect of interaction between the two proteins is relevant for human pathology.

Through administration of a cell-permeable peptide, Pro, for 2 weeks, we were able to reproduce ADAM10/SAP97 uncoupling *in vivo* in rodent brains. In Pro peptide, the short Tat sequence (11 amino acids) (Aarts *et al.*, 2002) is fused to the 32 amino acid sequence of the proline-rich domains of ADAM10, responsible for the direct binding to the SH3 domain of SAP97 (Marcello *et al.*, 2007). The peptide does not interfere with other protein complexes, implying that reported functional and behavioural modifications are not related to off-target effects.

Treatment of mice for 2 weeks with Pro peptide reduces ADAM10/SAP97 association and, consequently, ADAM10 localization to the postsynaptic membrane.

Specificity of the effects obtained after peptide treatment remains high with regard to the large number of ADAM10 substrates already described in the literature. This could be ascribed to either: (i) not all ADAM10 substrates are neuronally expressed; or (ii) our model is fully based on the uncoupling of the ADAM10/SAP97 complex in a very confined structure, the glutamatergic synapse, where both proteins are located. Again, among neuronal ADAM10 substrates, not all have spine localization.

Pro peptide treatment influences amyloid precursor protein metabolism, reducing α-secretase-mediated processing without affecting the processing of other synaptic, but developmentally relevant substrates, such as *N*-cadherin. The molecular rationale supporting the lack of ADAM10 cleavage of *N*-cadherin in the mature spine is at present not completely clear. Nonetheless, we can speculate that either clusterization of the enzyme or different accessibility of the substrates in mature spines compared with developmental stages could be relevant.

Importantly, there are no specific chemical inhibitors for basal ADAM10/α-secretase activity (Ludwig *et al.*, 2005). Pro peptide could therefore represent an appropriate tool to study the physiological role of ADAM10.

Exposing mice to Pro peptide for 2 weeks affects amyloid precursor protein metabolism, increasing amyloid precursor protein amyloidogenic cleavage with a modest but significant raise of Aβ release and of low-*n* Aβ aggregate production. This subtle increase in Aβ appears particularly promising when compared with data collected from studies in engineered animal models, where accumulation of soluble Aβ is normally reported in older animals, i.e. 9–13 months of age (Holcomb *et al.*, 1998; Oddo *et al.*, 2003*a*). Similarly, even in triple transgenic mice, Aβ oligomers can be revealed after 13 months of age (Oddo *et al.*, 2003*b*, 2006). Notably, in our conditions, the slight increase of both soluble Aβ and its low-*n* aggregates is evident after just 2 weeks of treatment. Although the low aggregation capability of rodent Aβ can be considered a limitation, ADAM10/SAP97 uncoupled animals still appear as a promising model to study early phases of Alzheimer's disease.

From a pathological point of view, hallmarks of Alzheimer's disease include extracellular amyloid plaques as well as intracellular neurofibrillary tangles (Selkoe, 2001). The latter trait is characteristic of human Alzheimer's disease but is not always present in amyloid models (Morrissette *et al.*, 2009), which in most cases do not even show tau hyperphosphorylation. For instance, mutant presenilin-1 mice crossed with mutant amyloid precursor protein mice fail to develop detectable neurofibrillary tangles (Holcomb *et al.*, 1998) and also in triple transgenic mice, lesions accumulate in an age-dependent fashion (Oddo *et al.*, 2003*a*). In ADAM10/SAP97 uncoupled mice, tau hyperphosphorylation, but not neurofibrillary tangles, was already evident after 2 weeks of treatment with Pro peptide, further supporting our hypothesis that these mice mimic early phases of pathology.

However, rather than deposition of amyloid plaques or neurofibrillary tangles, the most robust correlation in the staging of dementia and early Alzheimer's disease is the magnitude of synapse loss (Terry *et al.*, 1991; Scheff *et al.*, 2007). Spine loss and alterations in morphology have been linked to Aβ and its oligomeric aggregates in *in vivo* and *in vitro* studies (Lacor *et al.*, 2004; Shankar *et al.*, 2008; Wei *et al.*), suggesting a convergence between the main causes of Alzheimer's disease pathogenesis: amyloid cascade and synaptic alterations. In ADAM10/SAP97 uncoupled mice, we failed to adversely affect spine number and to alter spine morphology, probably because of the limited time of *in vivo* exposure to Aβ and its aggregates. The reasons for spine alterations in Alzheimer's disease remain controversial. Data emerging from a variety of transgenic mouse lines have pointed out a role for both low- and high-number oligomers (Jacobsen *et al.*, 2006). Their mechanism of action remains elusive, mostly because the vast majority of studies on the effects of Aβ oligomers on spine morphology have been carried out *in vitro* using *in vivo*-produced oligomers. A better knowledge of the mechanisms underlying spine deterioration in patients with Alzheimer's disease, which might involve effects of Aβ on cytoskeletal (Alvarez and Sabatini, 2007) and mitochondrial dysfunction (Hauptmann *et al.*, 2009), would be crucial for speculations on the reasons for the lack of spine alterations in our model. Studies with longer exposure to the Pro peptide might be helpful to dissect structural effects of ADAM10/SAP97 uncoupling.

Nevertheless, in ADAM10/SAP97 uncoupled mice, synaptic sufferance occurs prior to anatomical changes and is evident as a reorganization of the molecular composition of excitatory

glutamatergic synapse, with a selective reduction of the NR2A NMDA subunit. Recently, an effect of Aβ oligomers on NMDA receptor subunits has been reported, revealing an effect on NR2B trafficking and internalization (Snyder *et al.*, 2005; Lacor *et al.*, 2007). Our current findings on NR2A and spine morphology seem apparently contradictory, when compared with recent literature. This could be due to experimental discrepancies among studies, including different Aβ species, different stages of pathology or mice development at exposure and different concentrations and/or oligomerization state of Aβ (Billings *et al.*, 2005). The site of action of Aβ should also be considered, since intracellular and extracellular pools of Aβ may differently influence synaptic function, and the net outcome may depend on their dynamic relationship (Venkitaramani *et al.*, 2007). However, in agreement with previous studies (Cleary *et al.*, 2005), in our experimental conditions, NMDA subunit modifications at synaptic sites follow Aβ formation and accumulation, suggesting Aβ formation as the starting event of pathogenesis.

In our model, we described activity-dependent alterations of synaptic plasticity as well as an initial cognitive deficit in the Novel Object Recognition test, paralleling NR2A reduction. Interestingly, recent reports showed that long-term potentiation impairment in transgenic mice models of Alzheimer's disease depends on the age of the animals and, presumably, on Alzheimer's disease stage. For example, studies in ArcAb mice (where a form of Aβ more prone to yielding Aβ oligomers is expressed) revealed that long-term potentiation is impaired in mice of 3.5 and 7.5 months of age, but not in those of 1 month, probably because at this age, Aβ accumulation is not yet detectable (Knobloch *et al.*, 2007). In light of these previous data, lack of differences in hippocampal long-term potentiation in our model could be correlated to the early stage of Alzheimer's disease pathology revealed by our biochemical and morphological results. On the other hand, alterations in short-term synaptic plasticity found in our model have been documented in other Alzheimer's disease models. For example, double transgenic mice overexpressing the mutated form of amyloid precursor protein (APPK670N, M671L) and presenilin-1 (PS1M146V) exhibit enhanced synaptic fatigue, a form of short-term synaptic plasticity, at the Schaffer collateral-CA1 synapse (Zhang *et al.*, 2005). Intriguingly, because short-term synaptic changes are relevant in cognitive processes such as learning and memory, it is conceivable that alterations in the synaptic plasticity shown by our Alzheimer's disease model could be one leading cause of the impaired behavioural performances of these animals. Indeed, Pro peptide treated mice showed a marked impairment in the Novel Object Recognition test, which measures recognition memory and is heavily altered in Alzheimer's disease. This test relies on spontaneous animal behaviour without the need for stressor elements. Pro peptide treatment impairs memory consolidation within 24 h and rapidly interferes with the synaptic activity necessary for the stabilization of new memories.

In conclusion, our model can be used to study pathogenic consequences of a specific pathway of Alzheimer's disease pathogenesis, namely ADAM10/SAP97 disruption. Pro peptide treated animals manifest all characteristics of the early stages of Alzheimer's disease, i.e. increased Aβ production and presence of low-*n* aggregates, hyperphosphorylated tau and clear synaptic dysfunction as reflected by aberrant composition of NMDA receptors, altered activity-dependent plasticity and impaired behavioural performance. These manifestations occur prior to synapse loss and spine modifications and before the appearance of full pathological hallmarks, i.e. amyloid plaques and neurofibrillary tangles (Selkoe, 2008), highlighting the relevance of our model in studying the early stages of Alzheimer's disease.

Pro peptide strategy offers the unprecedented possibility to interfere with endogenous amyloid precursor protein processing in adult mice by neither overexpressing proteins derived from inherited forms of the disease nor altering developmental processes. Moreover, it can be useful to study the convergence as well as the temporal correlation of multiple neuropathological pathways, such as Aβ production and synaptic dysfunction and, eventually, to investigate new therapeutic strategies.

Funding

The research leading to these results has received funding from the European Union's Seventh Framework Programme (FP7 2007-2013; Grant Agreement n° PIAP-GA-2008-217902 to M.D.L.); by Fondazione Cariplo 2008 to M.D.L.; by Telethon-Italy (Grant Number GGP09196 to M.G.); by Compagnia di San Paolo to M.G. and by a fellowship from the Spanish Ministerio de Educación y Ciencia (Grant Number EX2006-0294 to H.V.). The authors are grateful to E. Zianni and A. Longhi for skilful technical work.

Supplementary material

Supplementary material is available at *Brain* online.

References

Aarts M, Liu Y, Liu L, Besshoh S, Arundine M, Gurd JW, et al. Treatment of ischemic brain damage by perturbing NMDA receptor- PSD-95 protein interactions. Science 2002; 298: 846–50.

Alvarez VA, Sabatini BL. Anatomical and physiological plasticity of dendritic spines. Annu Rev Neurosci 2007; 30: 79–97.

Billings LM, Oddo S, Green KN, McGaugh JL, LaFerla FM. Intraneuronal Abeta causes the onset of early Alzheimer's disease-related cognitive deficits in transgenic mice. Neuron 2005; 45: 675–88.

Braak H, Braak E. Neuropathological stageing of Alzheimer-related changes. Acta Neuropathol 1991; 82: 239–59.

Cleary JP, Walsh DM, Hofmeister JJ, Shankar GM, Kuskowski MA, Selkoe DJ, et al. Natural oligomers of the amyloid-beta protein specifically disrupt cognitive function. Nat Neurosci 2005; 8: 79–84.

Colledge M, Dean RA, Scott GK, Langeberg LK, Huganir RL, Scott JD. Targeting of PKA to glutamate receptors through a MAGUK-AKAP complex. Neuron 2000; 27: 107–19.

De Strooper B, Saftig P, Craessaerts K, Vanderstichele H, Guhde G, Annaert W, et al. Deficiency of presenilin-1 inhibits the normal cleavage of amyloid precursor protein. Nature 1998; 391: 387–90.

DeKosky ST, Scheff SW. Synapse loss in frontal cortex biopsies in Alzheimer's disease: correlation with cognitive severity. Ann Neurol 1990; 27: 457–64.

Epis R, Gardoni F, Marcello E, Genazzani A, Canonico PL, Di Luca M. Searching for new animal models of Alzheimer's disease. Eur J Pharmacol 2010; 626: 57–63.

Gamblin TC, Chen F, Zambrano A, Abraha A, Lagalwar S, Guillozet AL, et al. Caspase cleavage of tau: linking amyloid and neurofibrillary tangles in Alzheimer's disease. Proc Natl Acad Sci USA 2003; 100: 10032–7.

Gan WB, Grutzendler J, Wong WT, Wong RO, Lichtman JW. Multicolor "DiOlistic" labeling of the nervous system using lipophilic dye combinations. Neuron 2000; 27: 219–25.

Gardoni F, Bellone C, Cattabeni F, Di Luca M. Protein kinase C activation modulates alpha-calmodulin kinase II binding to NR2A subunit of N-methyl-D-aspartate receptor complex. J Biol Chem 2001; 276: 7609–13.

Gardoni F, Mauceri D, Fiorentini C, Bellone C, Missale C, Cattabeni F, et al. CaMKII-dependent phosphorylation regulates SAP97/NR2A interaction. J Biol Chem 2003; 278: 44745–52.

Gerlai R. Gene-targeting studies of mammalian behavior: is it the mutation or the background genotype? Trends Neurosci 1996; 19: 177–81.

Goate A, Chartier-Harlin MC, Mullan M, Brown J, Crawford F, Fidani L, et al. Segregation of a missense mutation in the amyloid precursor protein gene with familial Alzheimer's disease. Nature 1991; 349: 704–6.

Hardy JA, Higgins GA. Alzheimer's disease: the amyloid cascade hypothesis. Science 1992; 256: 184–5.

Hauptmann S, Scherping I, Drose S, Brandt U, Schulz KL, Jendrach M, et al. Mitochondrial dysfunction: an early event in Alzheimer pathology accumulates with age in AD transgenic mice. Neurobiol Aging 2009; 30: 1574–86.

Holcomb L, Gordon MN, McGowan E, Yu X, Benkovic S, Jantzen P, et al. Accelerated Alzheimer-type phenotype in transgenic mice carrying both mutant amyloid precursor protein and presenilin 1 transgenes. Nat Med 1998; 4: 97–100.

Jacobsen JS, Wu CC, Redwine JM, Comery TA, Arias R, Bowlby M, et al. Early-onset behavioral and synaptic deficits in a mouse model of Alzheimer's disease. Proc Natl Acad Sci USA 2006; 103: 5161–6.

Kim M, Suh J, Romano D, Truong MH, Mullin K, Hooli B, et al. Potential late-onset Alzheimer's disease-associated mutations in the ADAM10 gene attenuate {alpha}-secretase activity. Hum Mol Genet 2009; 18: 3987–96.

Klein WL, Krafft GA, Finch CE. Targeting small Abeta oligomers: the solution to an Alzheimer's disease conundrum? Trends Neurosci 2001; 24: 219–24.

Knobloch M, Konietzko U, Krebs DC, Nitsch RM. Intracellular Abeta and cognitive deficits precede beta-amyloid deposition in transgenic arcAbeta mice. Neurobiol Aging 2007; 28: 1297–306.

Lacor PN, Buniel MC, Chang L, Fernandez SJ, Gong Y, Viola KL, et al. Synaptic targeting by Alzheimer's-related amyloid beta oligomers. J Neurosci 2004; 24: 10191–200.

Lacor PN, Buniel MC, Furlow PW, Clemente AS, Velasco PT, Wood M, et al. Abeta oligomer-induced aberrations in synapse composition, shape, and density provide a molecular basis for loss of connectivity in Alzheimer's disease. J Neurosci 2007; 27: 796–807.

Lammich S, Kojro E, Postina R, Gilbert S, Pfeiffer R, Jasionowski M, et al. Constitutive and regulated alpha-secretase cleavage of Alzheimer's amyloid precursor protein by a disintegrin metalloprotease. Proc Natl Acad Sci USA 1999; 96: 3922–7.

Lau CG, Zukin RS. NMDA receptor trafficking in synaptic plasticity and neuropsychiatric disorders. Nat Rev Neurosci 2007; 8: 413–26.

Leonard AS, Davare MA, Horne MC, Garner CC, Hell JW. SAP97 is associated with the alpha-amino-3-hydroxy-5-methylisoxazole-4-propionic acid receptor GluR1 subunit. J Biol Chem 1998; 273: 19518–24.

Lesne S, Koh MT, Kotilinek L, Kayed R, Glabe CG, Yang A, et al. A specific amyloid-beta protein assembly in the brain impairs memory. Nature 2006; 440: 352–7.

Ludwig A, Hundhausen C, Lambert MH, Broadway N, Andrews RC, Bickett DM, et al. Metalloproteinase inhibitors for the disintegrin-like metalloproteinases ADAM10 and ADAM17 that differentially block constitutive and phorbol ester-inducible shedding of cell surface molecules. Comb Chem High Throughput Screen 2005; 8: 161–71.

Marcello E, Gardoni F, Mauceri D, Romorini S, Jeromin A, Epis R, et al. Synapse-associated protein-97 mediates alpha-secretase ADAM10 trafficking and promotes its activity. J Neurosci 2007; 27: 1682–91.

Morrissette DA, Parachikova A, Green KN, LaFerla FM. Relevance of transgenic mouse models to human Alzheimer disease. J Biol Chem 2009; 284: 6033–7.

Nash JE, Johnston TH, Collingridge GL, Garner CC, Brotchie JM. Subcellular redistribution of the synapse-associated proteins PSD-95 and SAP97 in animal models of Parkinson's disease and L-DOPA-induced dyskinesia. FASEB J 2005; 19: 583–5.

Oddo S, Caccamo A, Kitazawa M, Tseng BP, LaFerla FM. Amyloid deposition precedes tangle formation in a triple transgenic model of Alzheimer's disease. Neurobiol Aging 2003a; 24: 1063–70.

Oddo S, Caccamo A, Shepherd JD, Murphy MP, Golde TE, Kayed R, et al. Triple-transgenic model of Alzheimer's disease with plaques and tangles: intracellular Abeta and synaptic dysfunction. Neuron 2003b; 39: 409–21.

Oddo S, Caccamo A, Tran L, Lambert MP, Glabe CG, Klein WL, et al. Temporal profile of amyloid-beta (Abeta) oligomerization in an in vivo model of Alzheimer disease. A link between Abeta and tau pathology. J Biol Chem 2006; 281: 1599–604.

Postina R, Schroeder A, Dewachter I, Bohl J, Schmitt U, Kojro E, et al. A disintegrin-metalloproteinase prevents amyloid plaque formation and hippocampal defects in an Alzheimer disease mouse model. J Clin Invest 2004; 113: 1456–64.

Reiss K, Maretzky T, Ludwig A, Tousseyn T, de Strooper B, Hartmann D, et al. ADAM10 cleavage of N-cadherin and regulation of cell-cell adhesion and beta-catenin nuclear signalling. EMBO J 2005; 24: 742–52.

Sans N, Racca C, Petralia RS, Wang YX, McCallum J, Wenthold RJ. Synapse-associated protein 97 selectively associates with a subset of AMPA receptors early in their biosynthetic pathway. J Neurosci 2001; 21: 7506–16.

Scheff SW, Price DA, Schmitt FA, DeKosky ST, Mufson EJ. Synaptic alterations in CA1 in mild Alzheimer disease and mild cognitive impairment. Neurology 2007; 68: 1501–8.

Scheuner D, Eckman C, Jensen M, Song X, Citron M, Suzuki N, et al. Secreted amyloid beta-protein similar to that in the senile plaques of Alzheimer's disease is increased in vivo by the presenilin 1 and 2 and APP mutations linked to familial Alzheimer's disease. Nat Med 1996; 2: 864–70.

Seabold GK, Burette A, Lim IA, Weinberg RJ, Hell JW. Interaction of the tyrosine kinase Pyk2 with the N-methyl-D-aspartate receptor complex via the Src homology 3 domains of PSD-95 and SAP102. J Biol Chem 2003; 278: 15040–8.

Selkoe DJ. Alzheimer's disease: genes, proteins, and therapy. Physiol Rev 2001; 81: 741–66.

Selkoe DJ. Alzheimer's disease is a synaptic failure. Science 2002; 298: 789–91.

Selkoe DJ. Soluble oligomers of the amyloid beta-protein impair synaptic plasticity and behavior. Behav Brain Res 2008; 192: 106–13.

Shankar GM, Li S, Mehta TH, Garcia-Munoz A, Shepardson NE, Smith I, et al. Amyloid-beta protein dimers isolated directly from Alzheimer's brains impair synaptic plasticity and memory. Nat Med 2008; 14: 837–42.

Snyder EM, Nong Y, Almeida CG, Paul S, Moran T, Choi EY, et al. Regulation of NMDA receptor trafficking by amyloid-beta. Nat Neurosci 2005; 8: 1051–8.

Terry RD, Masliah E, Salmon DP, Butters N, DeTeresa R, Hill R, et al. Physical basis of cognitive alterations in Alzheimer's disease: synapse

loss is the major correlate of cognitive impairment. Ann Neurol 1991; 30: 572–80.

Vassar R, Bennett BD, Babu-Khan S, Kahn S, Mendiaz EA, Denis P, et al. Beta-secretase cleavage of Alzheimer's amyloid precursor protein by the transmembrane aspartic protease BACE. Science 1999; 286: 735–41.

Venkitaramani DV, Chin J, Netzer WJ, Gouras GK, Lesne S, Malinow R, et al. Beta-amyloid modulation of synaptic transmission and plasticity. J Neurosci 2007; 27: 11832–7.

Wei W, Nguyen LN, Kessels HW, Hagiwara H, Sisodia S, Malinow R. Amyloid beta from axons and dendrites reduces local spine number and plasticity. Nat Neurosci 2010; 13: 190–6.

Zhang H, Gong B, Liu S, Fa M, Ninan I, Staniszewski A, et al. Synaptic fatigue is more pronounced in the APP/PS1 transgenic mouse model of Alzheimer's disease. Curr Alzheimer Res 2005; 2: 137–40.

Zucker RS, Regehr WG. Short-term synaptic plasticity. Annu Rev Physiol 2002; 64: 355–405.